

# Determining the Minimal Required Radioactivity of $^{18}\text{F}$ -FDG for Reliable Semiquantification in PET/CT Imaging: A Phantom Study

Ming-Kai Chen<sup>1</sup>, David H. Menard III<sup>2</sup>, and David W. Cheng<sup>3</sup>

<sup>1</sup>Radiology and Biomedical Imaging, Yale University School of Medicine, New Haven, Connecticut; <sup>2</sup>Yale–New Haven Hospital, New Haven, Connecticut; and <sup>3</sup>Sidra Medical and Research Center, Doha, Qatar

In pursuit of as-low-as-reasonably-achievable (ALARA) doses, this study investigated the minimal required radioactivity and corresponding imaging time for reliable semiquantification in PET/CT imaging. **Methods:** Using a phantom containing spheres of various diameters (3.4, 2.1, 1.5, 1.2, and 1.0 cm) filled with a fixed  $^{18}\text{F}$ -FDG concentration of 165 kBq/mL and a background concentration of 23.3 kBq/mL, we performed PET/CT at multiple time points over 20 h of radioactive decay. The images were acquired for 10 min at a single bed position for each of 10 half-lives of decay using 3-dimensional list mode and were reconstructed into 1-, 2-, 3-, 4-, 5-, and 10-min acquisitions per bed position using an ordered-subsets expectation maximum algorithm with 24 subsets and 2 iterations and a gaussian 2-mm filter.  $\text{SUV}_{\text{max}}$  and  $\text{SUV}_{\text{avg}}$  were measured for each sphere. **Results:** The minimal required activity ( $\pm 10\%$ ) for precise  $\text{SUV}_{\text{max}}$  semiquantification in the spheres was 1.8 kBq/mL for an acquisition of 10 min, 3.7 kBq/mL for 3–5 min, 7.9 kBq/mL for 2 min, and 17.4 kBq/mL for 1 min. The minimal required activity concentration–acquisition time product per bed position was 10–15 kBq/mL-min for reproducible SUV measurements within the spheres without overestimation. Using the total radioactivity and counting rate from the entire phantom, we found that the minimal required total activity–time product was 17 MBq-min and the minimal required counting rate–time product was 100 kcps-min. **Conclusion:** Our phantom study determined a threshold for minimal radioactivity and acquisition time for precise semiquantification in  $^{18}\text{F}$ -FDG PET imaging that can serve as a guide in pursuit of achieving ALARA doses.

**Key Words:** PET; phantom; dosimetry; dose reduction; acquisition time; standard uptake value

**J Nucl Med Technol 2016; 44:26–30**

DOI: 10.2967/jnmt.115.165258

**T**here is a growing trend to minimize ionizing radiation exposure, particularly from diagnostic medical imaging

involving x-rays and internal radiation from administration of radionuclides. Recent evidence from a retrospective large-cohort study of over 178,600 U.K. residents who were exposed to radiation from CT scans in childhood found that a cumulative dose of more than 30 mGy to red bone marrow from as few as 5–10 head CT scans in children younger than 15 y carried a relative risk of 3.18 for leukemia as compared with a cumulative dose of less than 5 mGy. For brain cancer, a cumulative dose of 50–74 mGy to brain from as few as 2–3 head CT scans carried a relative risk of 2.82, as compared with those receiving a cumulative dose of less than 5 mGy (*1*). In a study of 680,000 Australians exposed to CT scans in childhood and adolescence, Mathews et al. found an incidence rate ratio of 1.24 for all cancers, with an observed dose–response relation of 0.16 per additional CT scan using an estimated average effective radiation dose of 4.5 mSv per scan (*2*).

$^{18}\text{F}$ -FDG PET/CT has been widely used for oncologic and cardiac imaging, with radiation exposure being derived from the injected dose of radiotracer and from the x-ray CT that is used for anatomic coregistration and attenuation correction. Previous studies suggested the effective dose from PET/CT to be in the range of 10–30 mSv, depending on the activity of  $^{18}\text{F}$ -FDG injected (0.02 mSv/MBq, according to International Commission on Radiological Protection publication 106) and the CT protocol (1–20 mSv) (*3–7*). In light of recent evidence that radiation exposure from medical imaging may carry a risk of cancer (*1,2,7*), we determined that a dose reduction from 555 MBq (15 mCi) to 370 MBq (10 mCi) does not affect  $\text{SUV}_{\text{max}}$  semiquantification or image quality (*8*). However, we suspected that dose could be reduced further without affecting SUV semiquantification or image quality using our standard PET data acquisition of 3 min per bed position. Using time-of-flight technology, Murray et al. (*9*) demonstrated biases introduced by low statistics. Although our scanner is time-of-flight-capable, we believe that time-of-flight SUVs may have limited usefulness given that far fewer scanners are time-of-flight-capable than not time-of-flight-capable. Furthermore, Murray et al. did not explore the threshold in counting statistics or report a practical parameter (e.g., minimum counting rate for each bed position) that can guide adjustments in PET acquisition time to maintain precision in SUVs. The aim of this study was to investigate the effect of counting rate and

Received Aug. 9, 2015; revision accepted Nov. 17, 2015.

For correspondence or reprints contact: David W. Cheng, Weill Cornell Medical College, Sidra Medical and Research Center, P.O. Box 26999, Doha, Qatar.

E-mail: [dcheng@sidra.org](mailto:dcheng@sidra.org)

Published online Jan. 14, 2016.

COPYRIGHT © 2016 by the Society of Nuclear Medicine and Molecular Imaging, Inc.

total accumulated counts on the precision and accuracy of semiquantification in order to determine the parameters needed to obtain PET/CT studies that can be directly compared with previous studies—an important (but often overlooked) consideration in maintaining continuity of care for clinicians.

## MATERIALS AND METHODS

A Discovery D-690 PET/CT scanner (GE Healthcare) was used. This scanner has a detection block of 54 ( $9 \times 6$ ) individual lutetium-orthosilicate (LYSO) crystals ( $4.2 \times 6.3 \times 25$  mm) coupled to a single square photomultiplier tube with 4 anodes (10). There are 24 rings of detectors (13,824 LYSO crystals), for an axial field of view of 157 mm and a transaxial field of view of 70 cm. The low-energy threshold is 425 keV, and the coincidence time window is 4.9 ns (10). The scanner operates in 3-dimensional mode only. The CT component of the scanner is a LightSpeed VCT with 912 channels  $\times$  64 rows, which allows full  $360^\circ$  scans with times ranging from 0.35 to 2 s and a slice thickness of  $64 \times 0.625$ ,  $32 \times 1.25$ ,  $16 \times 2.5$ ,  $8 \times 5$ , or  $4 \times 10$  mm (10).

We acquired PET/CT images using a standard Jaszczak phantom (model ECT/STD/P; Data Spectrum Corp.) modified with hollow spheres of various diameters (3.4, 2.1, 1.5, 1.2, 1.0, and 0.5 cm) that were filled with a fixed  $^{18}\text{F}$ -FDG concentration of 165 kBq/mL. The background radioactivity was 23.3 kBq/mL, for a target-to-background ratio of 7. Images were acquired for 10 min at a single bed position in list mode approximately every 2 h over a 20-h period of radioactive decay (Fig. 1). On an Advantage workstation (version 4.5; GE Healthcare)—and applying registered CT (120 kVp and 50–90 mA) for attenuation correction—the images were reconstructed into 1-, 2-, 3-, 4-, 5-, and 10-min acquisitions per bed position using an ordered-subsets expectation maximum algorithm with 24 subsets and 2 iterations and a gaussian 2-mm filter.

$\text{SUV}_{\text{max}}$  and  $\text{SUV}_{\text{avg}}$  were measured for each sphere by applying to the sphere a volume of interest having a threshold of 41% of the maximal value in the serial PET images. We also adjusted the size of the volume of interest according to the coregistered CT images to ensure that all volumes of interest were placed correctly. The SUV computation was derived from the radioactivity concentration (kBq/mL) divided by the total administered radioactivity within the phantom (kBq) and normalized to the total weight of the phantom (g). Because phantom weight was included, the SUV measurement was higher than the target-to-background ratio of 7. The coefficients of recovery were calculated by dividing the radioactivity in the PET images by the known activity as determined by a dose calibrator and correcting the decay back to the beginning time point. The variability in SUVs in each sphere at various time points was calculated against the SUV of the first 10-min acquisition in each sphere as the reference standard. An SUV deviation of  $\pm 10\%$  in comparison with the reference standard can be considered acceptable in accordance with the test–retest variability of 20% for  $^{18}\text{F}$ -FDG PET studies (11). The data were analyzed and plotted using Excel (version 2010; Microsoft).

## RESULTS

The coefficients of recovery for  $\text{SUV}_{\text{max}}$  calculated from our first acquisition were 0.97, 0.94, 0.79, 0.71, 0.45, and 0.17 for spheres with diameters of 3.4, 2.1, 1.5, 1.2, 1.0, and 0.5 cm, respectively. Because of severe partial-volume effects

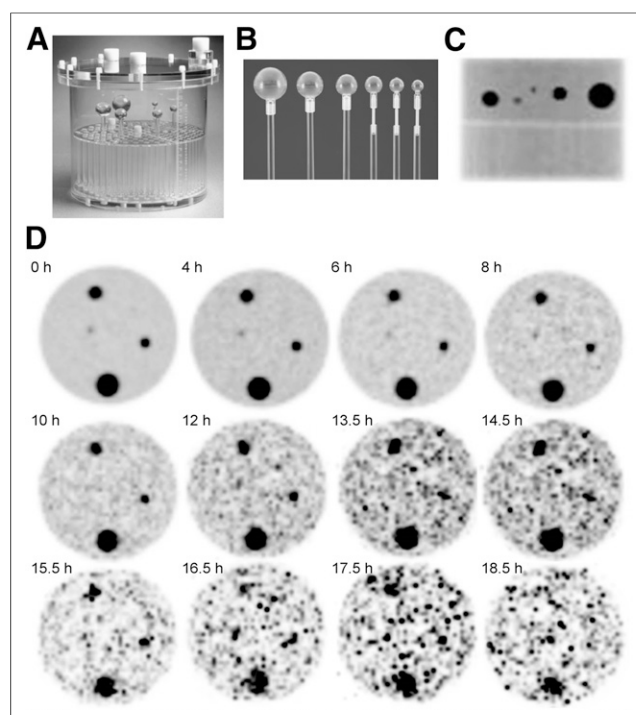


**FIGURE 1.** (A) Standard Jaszczak ECT phantom with solid spheres replaced by hollow spheres. (B) Hollow spheres with diameters of 3.4, 2.1, 1.5, 1.2, 1.0, and 0.5 cm. (C) Image of spheres filled with  $^{18}\text{F}$ -FDG (165 kBq/mL). (D) Transaxial reconstructed images at 0, 4, 6, 8, 10, 12, 13.5, 14.5, 15.5, 16.5, 17.5, and 18.5 h of decay (displayed in 3-min reconstruction).

on PET, the help of the CT images was needed to distinguish activity in the 0.5-cm sphere from background.

Figure 2A shows a dramatic overestimation of  $\text{SUV}_{\text{max}}$  at low radioactivity, up to 20.1 in the largest sphere (3.4 cm) as compared with the stable  $\text{SUV}_{\text{max}}$  range of 9–10. The overestimation could not be evaluated in smaller spheres because of severe partial-volume effects. Secondary to the partial-volume effects, the  $\text{SUV}_{\text{max}}$  for the same radioactivity concentration was much less in smaller spheres than in the largest sphere. Similarly, but to a lesser extent, Figure 2B demonstrates overestimation of  $\text{SUV}_{\text{avg}}$  in lower activity concentrations, up to 13.4 as compared with the reproducible  $\text{SUV}_{\text{avg}}$  range of 7–8 in the largest sphere. The overestimation of  $\text{SUV}_{\text{avg}}$  was not significant in smaller spheres.

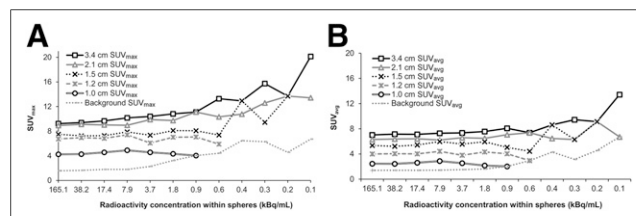


**FIGURE 2.** Impact of radioactivity concentration on  $\text{SUV}_{\text{max}}$  (A) and  $\text{SUV}_{\text{avg}}$  (B) in spheres of various sizes using 10-min acquisition. Radioactivity concentrations on x-axis correspond to acquisition time points of approximately 0, 4, 6, 8, 10, 12, 13.5, 14.5, 15.5, 16.5, 17.5, and 18.5 h.

Overestimation of  $SUV_{max}$  and  $SUV_{avg}$  was again seen in the background at lower radioactivity concentrations, with the  $SUV_{avg}$  range being less in smaller spheres than in the largest sphere at the same radioactivity concentration, possibly because of partial-volume effects (data not shown). Of note, the  $SUV_{max}$  range of 9–10 was calculated on the basis of the total weight of the phantom (including  $^{18}F$ -FDG solution and the phantom itself) and was higher than the presumed target-to-background ratio of 7. If we exclude the weight of the phantom,  $SUV_{max}$  should be close to 7. In fact,  $SUV_{max}$  for the ratio of the largest sphere to the background was approximately 7.

The minimal radioactivity concentration for reproducible  $SUV_{max}$  semiquantification was 1.8 kBq/mL for acquisitions of 10 min, 3.7 kBq/mL for 3–5 min, 7.9 kBq/mL for 2 min, and 17.4 kBq/mL for 1 min based on the acceptable deviation of SUV ( $\pm 10\%$ ) in all spheres in comparison with the reference standard (a 10-min acquisition at the beginning time point). The minimal activity for satisfactory visual assessment was 0.9 kBq/mL for acquisitions of 5 and 10 min, 1.8 kBq/mL for 3 and 4 min, 3.7 kBq/mL for 2 min, and 7.9 kBq/mL for 1 min. The minimal counting rates required from the entire phantom (or a single field of view) were 10 kcps for an acquisition of 10 min, 21 kcps for 3–5 min, 44 kcps for 2 min, and 98 kcps for 1 min. Figures 3A and 3B demonstrate the effect for the largest (3.4-cm-diameter) sphere.

Regarding the radioactivity concentration–acquisition time product per bed position, the minimal required value was 10–15 kBq/mL·min for reproducible SUV measurements ( $\pm 10\%$ ) (constrained to the smallest delineated sphere [1-cm diameter], with a lower value for larger spheres) without overestimation (Figs. 4B and 4C). When the counting rate from the entire phantom was used, the minimal required counting rate–acquisition time product was 100 kcps·min (data not shown).

We noticed that both  $SUV_{max}$  and  $SUV_{avg}$  were overestimated at low radioactivity concentrations at short acquisition times, with the overestimation being greater in larger spheres ( $\leq 300\%$  in the 3.4-cm sphere at the 1-min acquisition). This finding is likely attributable to a significant

buildup of noise, much of which would be due to the intrinsic contaminant radioactivity of  $^{176}Lu$  embedded within the crystal. The average counting rate without the phantom or external radioactivity, 1.1 kcps, was due to the room environment and the intrinsic properties of the scanner.

## DISCUSSION

In this study, we sought to determine the minimal radioactivity concentration that can reliably quantify SUV for various sizes of spheres, as surrogates for various sizes of  $^{18}F$ -FDG–avid lesions. Furthermore, by acquiring image sets over the 10 half-lives of decay, we could simulate lesions of the same size that have different  $^{18}F$ -FDG avidities (proportional to counting rates), allowing better understanding of the compensatory effects from increased total counts to improve counting statistics. We determined the minimal required counting rate for the entire phantom with various acquisition durations by calculating a radioactivity concentration (or counting rate)–acquisition time product. Using these data, we could estimate the minimal injected dose that achieves the required counting rate in the whole body and in various lesion sizes for an imaging protocol specifying a 3-min acquisition per bed position. It may be possible to further reduce the injected dose, and hence the radiation exposure and absorbed dose, by extending the acquisition to 4–5 min or longer. Conversely, if a patient cannot tolerate a 3-min acquisition per bed position, the model can be used to estimate how much higher a dose is needed to allow for a shorter acquisition time.

Version 1.0 of the European Association of Nuclear Medicine procedure guideline for PET imaging of tumors recommends an  $^{18}F$ -FDG dose of 5 MBq/kg of body weight ( $\pm 10\%$ ) for 2-dimensional scans and 2.5 MBq/kg for 3-dimensional scans based on a 5-min acquisition per bed position and an overlap of less than 25% between bed positions (12). Alternate dosing for different scanning durations per bed position can be calculated using equations for varying body weight (MBq/kg), for 2- versus 3-dimensional scans, and for varying bed overlap (25% vs 50%) on scanners equipped with lutetium oxyorthosilicate (LSO), LYSO, or germanium oxyorthosilicate crystals (12). It was found that the  $^{18}F$ -FDG activity could be as low as 6.9 times the body weight per acquisition (minutes per bed position), or 2.3 MBq/kg for a 3-min acquisition per bed position using a bed position overlap of 50% (12). According to our phantom data, the minimal required total activity at the time of imaging for reproducible semiquantification is 3.6 MBq in a 9-kg phantom, or 0.4 MBq/kg for an acquisition of 3 min per bed position. Taking into account urinary excretion of 20%–25% of activity (6,13,14) and 1 h of decay during distribution of uptake after injection, the weight-based injected dose may translate to approximately 0.8 MBq/kg using a 3-min-per-bed-position acquisition in the D-690 scanner. Because our estimates were made assuming ideal parameters, more conservative adjustments may be needed for heavier patients.

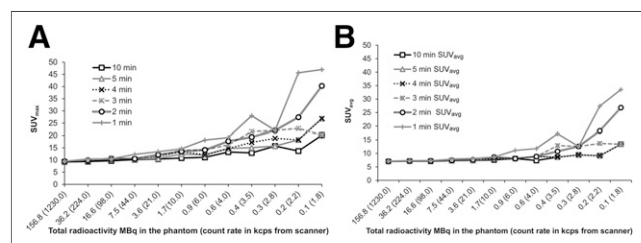


**FIGURE 3.** Impact of total radioactivity on  $SUV_{max}$  (A) and  $SUV_{avg}$  (B) in 3.4-cm sphere at various acquisition times.  $SUV_{max}$  is significantly overestimated at earlier acquisitions (47 at 1-min acquisition compared with 9–10 at later acquisitions). Likewise,  $SUV_{avg}$  is overestimated at earlier acquisitions (33.6 at 1-min acquisition compared with 7–8 at later acquisitions). Counting rates are not corrected for random counts or dead time.



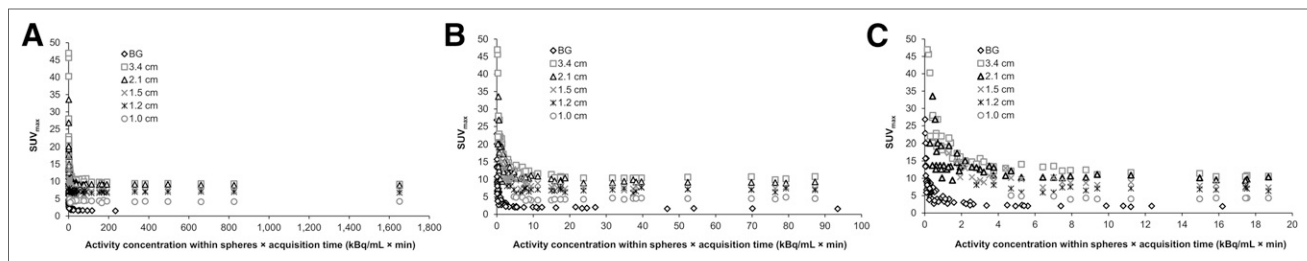


**FIGURE 4.** Use of radioactivity concentration–acquisition time product to determine reproducibility of  $SUV_{max}$  in spheres of various sizes.  $SUV_{max}$  is overestimated within a low range of concentration–time product. Data for typical (A) and expanded (B and C) x-axes are shown.

Previous studies on optimal injected activity and acquisition have focused on noise-equivalent counting rate and systematic performance (15–19). However, clinicians may use the reproducibility of SUV measurements as a more sensitive guide to image quality in assessing direct comparability between initial and follow-up (treatment response) PET images. Any reduction in the injected dose from published recommended protocols or guidelines will translate into a lower cumulative dose and better long-term survival for each patient, which will be especially important for patients requiring 3 or 4 PET/CT studies a year.

Overestimation of  $SUV_{max}$  and  $SUV_{avg}$  in spheres containing low radioactivity concentrations has been observed and may be explained through low counting statistics and the intrinsic (background) radioactivity of the LYSO crystal. Overestimation of  $SUV_{max}$  has been reported from noisier imaging using only a small portion of total counts in a respiration-gated study (20). However, overestimation of  $SUV_{avg}$  may also be explained by factors other than noise buildup alone. The LYSO crystal, similar to the LSO crystal, is intrinsically radioactive because of the presence of  $^{176}\text{Lu}$  (2.6%) in nature.  $^{176}\text{Lu}$  decays by  $\beta^-$  (mean energy, 420 keV) followed by prompt emission of  $\gamma$ -rays at 307, 202, and 88 keV.  $\beta^-$ -particles are absorbed within the crystal of origin, whereas  $\gamma$ -rays are detected by a different crystal. Hence, this intrinsic radioactivity can produce up to 1 million counts per second as detected by the entire scanner, with a total random coincidence rate of 1,600 cps in a 350- to 650-keV acceptance window, and falsely contributes a true coincidence rate of approximately 600 cps in an LSO scanner (21,22). The intrinsic rate can be reduced from 940 cps in a 250- to 750-keV energy window to less than 2 cps in a 400- to 750-keV window as demonstrated in an LSO-based small-animal PET scanner (23). The D-690 scanner has set the lower threshold to 425 keV, and the significantly reduced reported intrinsic rate of about 1 cps (10) can be considered negligible in clinical settings but not at low counting rates such as in lesions with low  $^{18}\text{F}$ -FDG avidity. Other explanations may include suboptimal scanner calibration at these low counting rates, inaccurate dead-time correction at these low counting rates, or a suboptimal reconstruction algorithm. Investigations using scanners by other vendors at low counts may further support our results and conclusions.

In a recent clinical publication (8), we observed stabilization of SUVs through counting statistics with longer acquisition times. Although our clinical protocol limited us to a maximum of 3 min per bed position, the counting rates from the lesions were more than adequate to provide good precision in our SUVs, which allayed our concerns over whether our injected dose was sufficient for good contrast between pathologic findings and physiologic biodistribution in the entire body. Schwartz et al. (24) demonstrated the intrinsic behavior of SUVs using a large  $^{68}\text{Ge}$ -phantom with a half-life of 271 d that enabled 30 runs of up to 30 min each. With the decay of our  $^{18}\text{F}$ -FDG phantom over 10 half-lives, we were able to test the bounds within which SUVs will remain precise. In performing this 20-h-long experiment, our most arduous effort was in maintaining a valid comparison of an individual SUV between time points (25,26). Our data trend agreed with the findings of Schwartz et al. (24), giving us confidence that we have accounted for the intrinsic factors in our results and can draw valid conclusions outside their range (37 kBq/mL of  $^{18}\text{F}$ -FDG). Given the short half-life of  $^{18}\text{F}$ -FDG (only 109 min) and the unrealistic expectation that a patient will lie still for longer than 3–4 min per bed position, the practice of ALARA (as low as reasonably achievable) in the clinical setting must be balanced by achieving a sufficient counting rate (and acquiring adequate total counts for good statistics) within 3–4 min per field of view. Otherwise, comparability between studies may come into question, especially when SUVs are used to determine changes in response to treatment. Because the sensitivity of detecting a lesion is directly dependent on the target-to-background ratio, qualitative assessments—regardless of whether the scan is for initial staging or for restaging—depend solely on the reconstructed image on the screen, the quality of which is a direct reflection of the underlying counting statistics.

Our work can be expanded into an exploration of various reconstruction settings (pixel sizes, filters, subsets, and iterations) with varying tumor-to-background ratios using an anthropomorphic phantom. Limitations of this work include the need to validate our thresholds on clinical patients, especially since our thresholds are lower than the current recommendations of the European Association of Nuclear Medicine. We anticipate that the clinical protocol will require a higher administered dose because of physiologic

urinary excretion of  $^{18}\text{F}$ -FDG; hence, we tried to estimate the thresholds from counting rates during the PET acquisition and to be flexible with acquisition times in order to obtain good statistics. To our knowledge, this approach has not been explored or reported as a way to implement ALARA standards in patients and nuclear medicine staff while maintaining comparable SUVs. Murray et al. (9) proposed lowering injected doses for response-to-chemotherapy studies but not for baseline and end-of-treatment studies. ALARA can extend to all patients at all times, and the results, SUVs in particular, should be directly comparable in all studies.

## CONCLUSION

Our phantom study determined the importance of counting statistics to the overall quality and usefulness of a PET/CT study. Our quantitative approach ensures direct comparability between longitudinal studies and enables determination of the minimum dose required to achieve ALARA standards so as to minimize the risk of secondary cancer over a patient's lifetime.

## DISCLOSURE

No potential conflict of interest relevant to this article was reported.

## ACKNOWLEDGMENT

We thank Chi Liu, PhD, for his suggestions during preparation of the manuscript.

## REFERENCES

- Pearce MS, Salotti JA, Little MP, et al. Radiation exposure from CT scans in childhood and subsequent risk of leukaemia and brain tumours: a retrospective cohort study. *Lancet*. 2012;380:499–505.
- Mathews JD, Forsythe AV, Brady Z, et al. Cancer risk in 680,000 people exposed to computed tomography scans in childhood or adolescence: data linkage study of 11 million Australians. *BMJ*. 2013;346:f2360.
- Radiation dose to patients from radiopharmaceuticals: addendum 3 to ICRP publication 53—ICRP publication 106, approved by the commission in October 2007. *Ann ICRP*. 2008;38:1–197.
- Brix G, Lechel U, Glatting G, et al. Radiation exposure of patients undergoing whole-body dual-modality  $^{18}\text{F}$ -FDG PET/CT examinations. *J Nucl Med*. 2005;46:608–613.
- Gelfand MJ. Dosimetry of FDG PET/CT and other molecular imaging applications in pediatric patients. *Pediatr Radiol*. 2009;39(suppl 1):S46–S56.
- Hays MT, Watson EE, Thomas SR, Stabin M. MIRD dose estimate report no. 19: radiation absorbed dose estimates from  $^{18}\text{F}$ -FDG. *J Nucl Med*. 2002;43:210–214.
- Huang B, Law MW, Khong PL. Whole-body PET/CT scanning: estimation of radiation dose and cancer risk. *Radiology*. 2009;251:166–174.
- Cheng DW, Ersahin D, Staib LH, Della Latta D, Giorgetti A, d'Errico F. Using SUV as a guide to  $^{18}\text{F}$ -FDG dose reduction. *J Nucl Med*. 2014;55:1998–2002.
- Murray I, Kalemis A, Glennon J, et al. Time-of-flight PET/CT using low-activity protocols: potential implications for cancer therapy monitoring. *Eur J Nucl Med Mol Imaging*. 2010;37:1643–1653.
- Bettinardi V, Presotto L, Rapisarda E, Picchio M, Gianolli L, Gilardi MC. Physical performance of the new hybrid PETCT Discovery-690. *Med Phys*. 2011;38:5394–5411.
- Frings V, van Velden FH, Velasquez LM, et al. Repeatability of metabolically active tumor volume measurements with FDG PET/CT in advanced gastrointestinal malignancies: a multicenter study. *Radiology*. 2014;273:539–548.
- Boellaard R, O'Doherty MJ, Weber WA, et al. FDG PET and PET/CT: EANM procedure guidelines for tumour PET imaging—version 1.0. *Eur J Nucl Med Mol Imaging*. 2010;37:181–200.
- Dowd MT, Chen CT, Wendel MJ, Faulhaber PJ, Cooper MD. Radiation dose to the bladder wall from 2- $^{18}\text{F}$ fluoro-2-deoxy-D-glucose in adult humans. *J Nucl Med*. 1991;32:707–712.
- Ruotsalainen U, Suhonen-Polvi H, Eronen E, et al. Estimated radiation dose to the newborn in FDG-PET studies. *J Nucl Med*. 1996;37:387–393.
- Everaert H, Vanhove C, Lahoutte T, et al. Optimal dose of  $^{18}\text{F}$ -FDG required for whole-body PET using an LSO PET camera. *Eur J Nucl Med Mol Imaging*. 2003;30:1615–1619.
- Inoue K, Kurosawa H, Tanaka T, Fukushi M, Moriyama N, Fujii H. Optimization of injection dose based on noise-equivalent count rate with use of an anthropomorphic pelvis phantom in three-dimensional  $^{18}\text{F}$ -FDG PET/CT. *Radiol Phys Technol*. 2012;5:115–122.
- Lartizien C, Comtat C, Kinahan PE, Ferreira N, Bendriem B, Trebussen R. Optimization of injected dose based on noise equivalent count rates for 2- and 3-dimensional whole-body PET. *J Nucl Med*. 2002;43:1268–1278.
- Watson CC, Casey ME, Bendriem B, et al. Optimizing injected dose in clinical PET by accurately modeling the counting-rate response functions specific to individual patient scans. *J Nucl Med*. 2005;46:1825–1834.
- Masuda Y, Kondo C, Matsuo Y, Uetani M, Kusakabe K. Comparison of imaging protocols for  $^{18}\text{F}$ -FDG PET/CT in overweight patients: optimizing scan duration versus administered dose. *J Nucl Med*. 2009;50:844–848.
- Liu C, Alessio A, Pierce L, et al. Quiescent period respiratory gating for PET/CT. *Med Phys*. 2010;37:5037–5043.
- Erdi YE, Nehmeh SA, Mulnix T, Humm JL, Watson CC. PET performance measurements for an LSO-based combined PET/CT scanner using the National Electrical Manufacturers Association NU 2-2001 standard. *J Nucl Med*. 2004;45:813–821.
- Watson CC, Casey ME, Eriksson L, Mulnix T, Adams D, Bendriem B. NEMA NU 2 performance tests for scanners with intrinsic radioactivity. *J Nucl Med*. 2004;45:822–826.
- Goertzen AL, Stout DB, Thompson CJ. A method for measuring the energy spectrum of coincidence events in positron emission tomography. *Phys Med Biol*. 2010;55:535–549.
- Schwartz J, Humm JL, Gonen M, et al. Repeatability of SUV measurements in serial PET. *Med Phys*. 2011;38:2629–2638.
- Boellaard R, Krak NC, Hoekstra OS, Lammertsma AA. Effects of noise, image resolution, and ROI definition on the accuracy of standard uptake values: a simulation study. *J Nucl Med*. 2004;45:1519–1527.
- Keyes JW Jr. SUV: standard uptake or silly useless value? *J Nucl Med*. 1995;36:1836–1839.



## Determining the Minimal Required Radioactivity of $^{18}\text{F}$ -FDG for Reliable Semiquantification in PET/CT Imaging: A Phantom Study

Ming-Kai Chen, David H. Menard III and David W. Cheng

*J. Nucl. Med. Technol.* 2016;44:26-30.

Published online: January 14, 2016.

Doi: 10.2967/jnmt.115.165258

---

This article and updated information are available at:

<http://tech.snmjournals.org/content/44/1/26>

---

Information about reproducing figures, tables, or other portions of this article can be found online at:


<http://tech.snmjournals.org/site/misc/permission.xhtml>

Information about subscriptions to JNMT can be found at:

<http://tech.snmjournals.org/site/subscriptions/online.xhtml>

*Journal of Nuclear Medicine Technology* is published quarterly.  
SNMMI | Society of Nuclear Medicine and Molecular Imaging  
1850 Samuel Morse Drive, Reston, VA 20190.  
(Print ISSN: 0091-4916, Online ISSN: 1535-5675)

© Copyright 2016 SNMMI; all rights reserved.

 SOCIETY OF  
NUCLEAR MEDICINE  
AND MOLECULAR IMAGING